Periodical structures induced by femtosecond laser on nickel in air

C. ALBU[a,b,*], C. LUCULESCU[a], M. ZAMFIRESCU[a]
[a]*National Institute for Laser, Plasma and Radiation Physics, Atomistilor 409, 077125 Magurele, Romania*
[b]*University of Bucharest, Faculty of Physics, Atomistilor Str. 405, P. O. Box MG-11, 077125 Magurele-Bucharest, Romania*

Ripples or periodical structures are obtained on nickel films by irradiation with femtosecond laser pulses working at both fundamental (775 nm) and frequency doubled (387 nm) wavelengths in air. Depending on the irradiation conditions, such as laser fluence, number of laser pulses or laser wavelength, different morphology and ripples periods has been obtained: Low Spatial Frequency LIPSS (LSFL) with a periodicity of about 240 to 650 nm, and High Spatial Frequency LIPSS (HSFL) with a periodicity from about 100 to 190 nm. Our experimental observations are complemented by calculated ripples period predicted by the classical interference theory and surface plasmon theory.

(Received October 8, 2013; accepted May 15, 2014)

Keywords: Femtosecond laser, LIPSS, Nickel

1. Introduction

Ripples or laser-induced periodic surface structures (LIPSS) have been observed near the ablation threshold of materials since the beginning of laser processing [1]. Arrays of periodic linear structures with some bifurcations are observed on many types of materials such as metals, semiconductors or dielectrics [2-6]. Spatial period of clasical LIPSS structure are usually comparable or slightly smaller than the laser wavelength ($\Lambda = \lambda$). These structures are known as low-spatial frequency LIPSS (LSFL). Further experimental studies reported another type of LIPPS structures known as high-spatial frequency LIPSS (HSFL) with the spatial period in some cases λ /10 [7]. Usually, the direction of LSFL is perpendicular to the polarization of incident laser light and the direction of HSFL is parallel to the laser polarization direction.

The most popular theory that describes the formation of LSFL structures is based on the interference model [8]. This theory interprets the formation of ripples structure as a result of interference between the incident laser beam and surface-scattered waves. Such model cannot be applied for HSFL, due to their period much smaller then laser wavelength. For these types of structures were proposed other formation mechanisms such as self-organization or excitation of surface plasmons (SPs) [9]. All these models cannot give a complete explanation of LIPPS, their formation mechanism is still under debate. Even if the ripples formation is not completely understood such periodical surface structures can be used for color marking of metals or substrate for cells growth [10, 11]. More recently, T.Y. Hwang [12] demonstrated that fs laser-induced surface structures on nickel can change the optical properties of the surfaces, therefore is well suited for use as a solar absorber surface. For all these applications a better control of the nanostructures morphology is required and the experimental approach plays an important role on the investigation of mechanism formation of ripples.

In this work we performed an experimental study on the formation of periodical structures on nickel films irradiated by femtosecond laser pulses working at both fundamental (775 nm) and frequency doubled (387 nm) wavelengths in air. Depending on the irradiation conditions, such as laser fluence, number of laser pulses or laser wavelength, different morphology and ripples periods has been obtained.

The experimental results are complemented by calculated ripples period predicted by the classical interference theory and surface plasmon theory.

2. Experimental

Experimental set-up is presented in Fig. 1. To processing the metallic sample, an linearly polarized laser pulses from a Ti:Sapphire regenerative amplifier laser system (Clark CPA-2101) was used. The pulse duration of this laser source is 200 fs and repetition rate 2 kHz. The fundamental wavelength at 775 nm was frequency doubled (387.5 nm) by a BBO nonlinear crystal. The spatial profile of the laser beam is nearly Gaussian. The irradiation was performed under normal incidence (θ=0^o) and the processing direction was parallel to the laser polarization direction. Scanning laser beam across the sample in NIR

experiments was performed by a two mirror galvano-scanner system. The focusing optics was an f-theta lens with focal length of 100 mm. The calculated diameter of the focused laser beam was 35 μm at $1/e^2$ from the maximum intensity. For UV experiments, the second harmonic from the BBO crystal was focused by a lens with 75 mm focal length. The calculated diameter of the focused spot diameters in air was 14 μm. Since the samples were processed with laser fluences near the ablation threshold, the laser modified surface spot has a diameter of less than 10 μm for UV and 12 μm for NIR experiments [13]. In order to completely cover the sample surface with LIPSS nanostructures, surfaces of about 1 mm^2 were processed by scanning the samples sequentially, line by line, at different scanning speeds from 0.1 to 10 mm/s and laser fluence varied from 0.05 to 0.35 J/cm^2. The thickness of metallic films is 200 nm and was deposited by electron beam evaporation technique on Si (111). The samples ware cleaned before and after laser processing, in ultrasonic bath for 5 minutes in acetone and de-ionized water. Characterization of morphological changes of the laser-modified surface was performed using a Scanning Electron Microscopy (SEM) and Atomic Force Microscopy (AFM). For quantitative evaluation of the average spatial LIPSS period Λ, two-dimensional Fourier transform (2D-FT) of the SEM images was used.

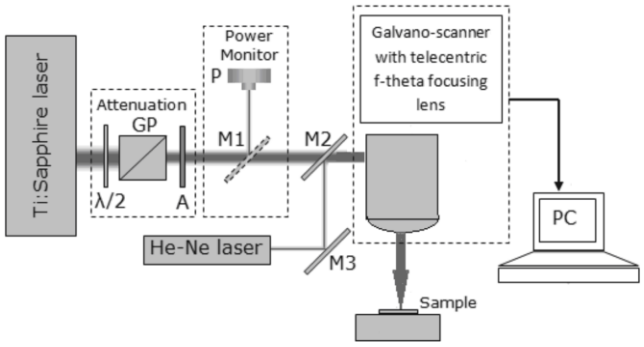

Fig.1. Schematic representation of the experimental set-up.

3. Results and discussion

SEM images of morphological evolution of periodic surface structures on nickel surface in air at 775 nm laser wavelengths are presented Fig. 2. The LIPSS structures are shown for different laser fluence and the same scanning speed. A clear dependence of the LIPSS morphologies with laser fluence is observed. For low laser fluence ($F \approx 0.18$ J/cm^2), the samples start to be affected by femtosecond laser pulses and over the entire surface can be observed few HSFL structures (Fig. 2a). The average spatial LIPSS period Λ is estimated from the 2D-FT image (not shown here). The periodicities have been measured between 160 and 190 nm. The ripples orientation is paralell to the laser polarization and is independent to the scanning direction, as commonly observed [14].

Increasing the laser fluence ($F \approx 0.20$ J/cm^2), both HSFL and LSFL ripples structures start to develop at the surface of the material (Fig. 2b). The ripples orientation is parallel to the laser polarization in HSFL case and perpendicular to the laser polarization in LSFL case. Periodicity of this LIPSS structures varies between 190 nm and 350 nm. Further increases in laser fluence ($F \approx 0.22$ J/cm^2) leads to LSFL type structures obtained on the sample surface (Fig. 2c). Periodicity of these structures is about 600 nm and orientation is perpendicular to the laser polarization.

The influence of the laser scanning speed on structures morphology was also investigated. For high scanning speed (over 8mm/s) and low laser fluence the sample surface is almost not affected by the femtosecond laser pulses. Decreasing the scan speed (4 mm/s or less) HSFL structures begin to appear on the surface sample. For intermediate scanning speed (below 6mm/s) mixed ripples structures are visible and transition from HSFL to LSFL type occurs on the sample surface. When scan speed increases above 6 mm/s, LSFL structures are obtained. Same result was obtained for high laser fluence and scanning speeds greater than 8 mm/s. When scan speed decreases down to 2 mm/s the sample surface is partially removed by laser ablation. For even lower scanning speeds the metal film is completely removed from the substrate.

After AFM investigation (Fig. 3), the depth of the created structures was determined. Depending on the laser fluence the average height of the formed structures was between 90-120 nm for $F \approx 0.18$ J/cm^2 and 180-220 nm for $F \approx 0.22$ J/cm^2.

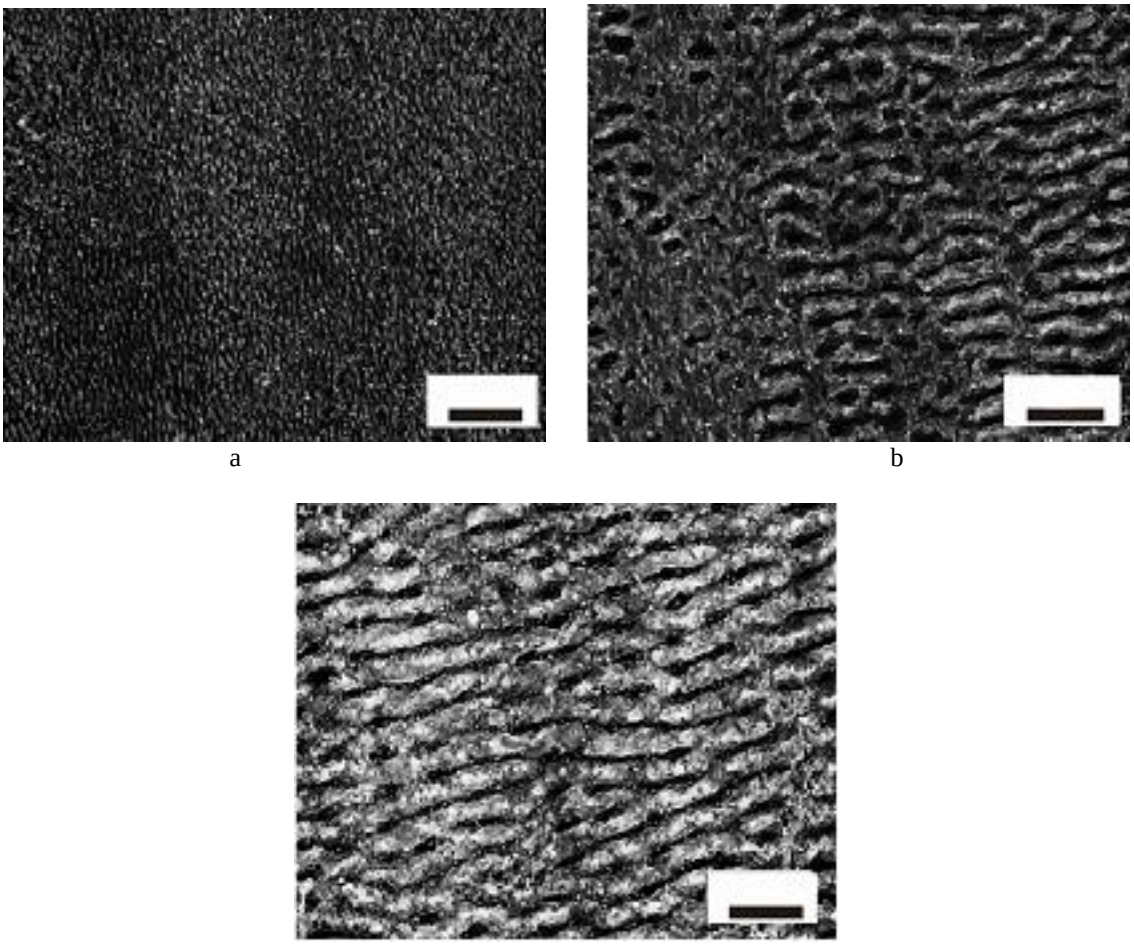

a b c

Fig. 2. LIPSS produced on Ni sample using 775 nm laser wavelength, same scan speed (v = 4 mm/s) and different laser fluence: a) F ≈ 0.18 J/cm^2; b) F ≈ 0.20 J/cm^2, c) F ≈ 0.22 J/cm^2. Scale bar: 1 µm.

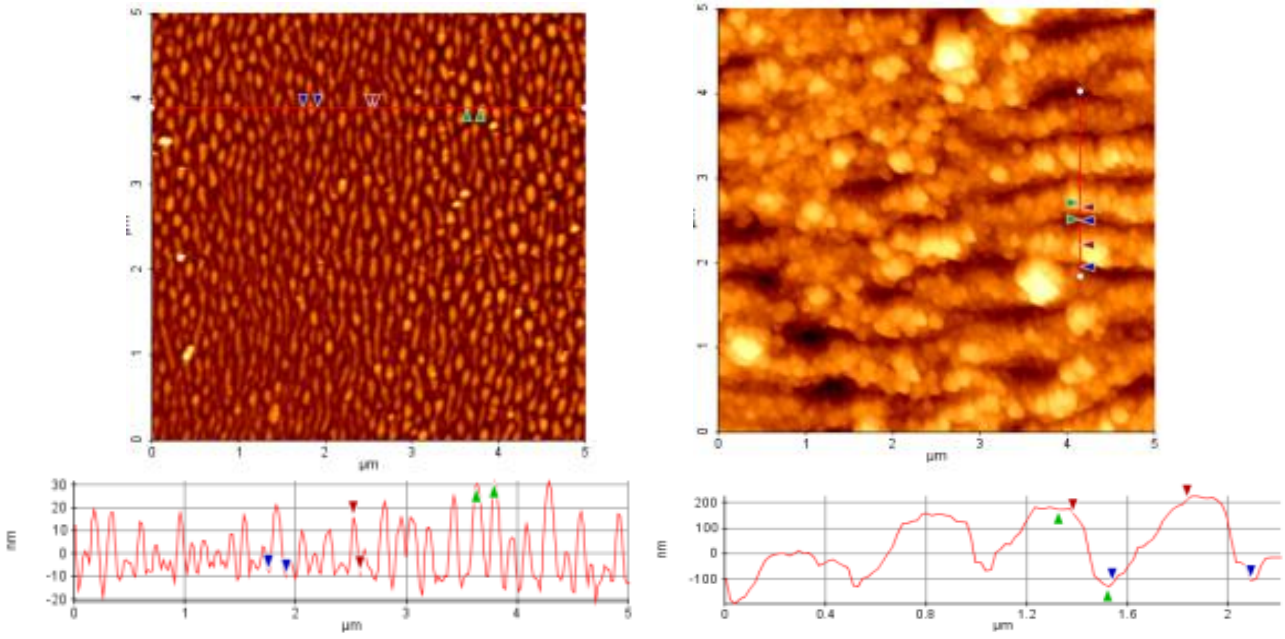

a b

Fig. 3. AFM investigation on nickel sample for Λ_{775} , scan speed (v = 4 mm/s) and different laser fluence a) F ≈ 0.18 J/cm^2, h= 90-120 nm; b) F ≈ 0.22 J/cm^2, h= 180-220 nm.

Fig. 4 shows the SEM images of morphological evolution of periodic surface structures for UV laser irradiation. For low laser fluence ($F \approx 0.05$ J/cm^2), the samples surface start to be affected and HSFL structures can be seen (Fig. 4a). The average spatial LIPSS period Λ is 90 nm up to 120 nm. For higher laser fluence ($F \approx 0.10$ J/cm^2), periodicities of LSFL structures is between 200 and 240 nm (Fig. 4b). The ripples orientation is parallel to the laser polarization in HSFL case and perpendicular to the laser polarization in LSFL case.

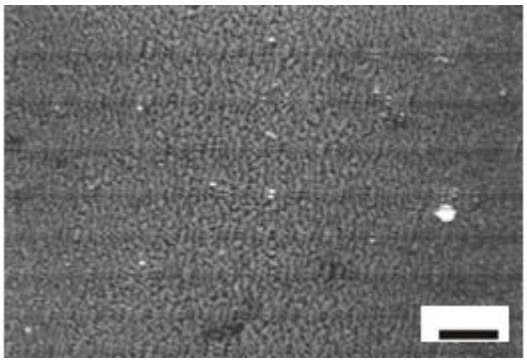

a

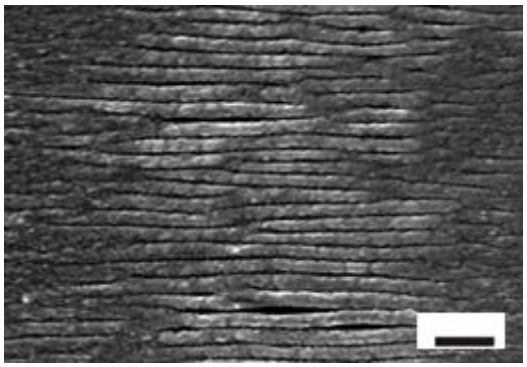

b

Fig. 4. Periodic surface structures produced on sample surface using 387 nm laser wavelength, same scan speed (v = 1 mm/s) and different laser fluence: a) $F \approx 0.05$ J/cm^2; b) $F \approx 0.10$ J/cm^2. Scale bar: 1 μm.

The formation mechanism of LIPSS was for many years attributed to the interference of the incident laser with the surface scattered waves, with period given by $\Lambda = \lambda / n_\lambda$ (n_λ is the refractive index of materials as a function of λ). However, the values obtained from our measurements are slightly different from the values predicted by the classical interference theory. The formation mechanism and period of LIPSS could be better explained within the surface plasmon theory where the period of ripples can be related to the surface plasmon wavelength. The interference between the incident laser light and the excited surface plasmons wave created at the dielectric-material interface will causes a periodic intensity variation on surface and consequently a periodical thermal gradient. The melted material moves from the hot regions to colder region (Marangoni effect), then periodical structures are formed by a self-organized process [15].

The experimental LIPSS periods measured, are compared with the values of the SP wavelength and with the relation given by the interference model $\Lambda = \lambda_0 / n_\lambda$, where n_λ is the refractive index of materials as a function of λ. The SPs wavelength is

$$\lambda_{SP} = \lambda_0 \mathrm{Re}\left[\left(\frac{\varepsilon_d \varepsilon_m}{\varepsilon_d + \varepsilon_m}\right)^{1/2}\right],$$

where λ_0 is laser wavelength ε_d refers to the permittivity of the dielectric medium, and $\varepsilon_m = \varepsilon_r + i\,\varepsilon_i$ is the complex dielectric constant of the metal [16].

Taking into account the complex dielectric permittivity ε of Ni with $Re\{\varepsilon\} = -12.67$ and $Im\{\varepsilon\} = 20.94$ at $\lambda \approx 775$ nm, the SP wavelength for air/metal interface is $\lambda_{SP} \approx 774$ nm. This theoretical value is higher compared to the measured LIPSS period $\Lambda_{775} = 650$ nm and slightly lower than the laser wavelength. The measured and estimated LIPSS periods at both laser wavelengths of 775 nm respectively 387 nm are listed in Table 1.

Table 1. Comparison between experimental and calculated LIPSS period Λ based on the classical interference theory ($\Lambda = \lambda / n_\lambda$) and surface plasmon theory ($\Lambda = \lambda_{SP}$).

Material		λ_0=775 nm			λ_0=387 nm		
		Experimental periodicity Λ (nm)	λ_0/n_λ (nm)	λ_{SP} (nm)	Experimental periodicity Λ (nm)	λ_0/n_λ (nm)	λ_{SP} (nm)
Nickel	HSFL	160-350	320	743	90-190	240	305
	LSFL	600-650			200-300		

We observe large differences between the experimental periods and the values given by the interference model. The experimental results are closer to the values given by the SPs wavelengths, the slight differences between the measured and theoretically predicted LIPSS period was explained within the Drude-Lorentz model, as a transient modification of the dielectric permittivity due to the ultrashort laser excitation [17].

4. Conclusions

Large area of nano-structured Ni surface were obtained by laser irradiation. The control parameters for nanostructuring are the laser fluences, scanning speed and laser wavelength. The LIPSS period is controlled in the range of 100 nm to 650 nm Depending on the laser fluence, the average height of the formed structures was between 90-220 nm. We observe differences between experimental measurements and the actual theories: large differences between the experimental periods and the values given by the interference model and small differences for the values given by the SPs wavelengths. The differences between the measured and theoretically predicted LIPSS period could be explained by the transient modification of the dielectric permittivity due to the ultrashort laser excitation.

Acknowledgements

This work was supported by a grant of the Ministry of National Education, CNCS – UEFISCDI, project number PN-II-ID-PCE-2012-4-0539.

References

[1] M. Birnbaum, J. Appl. Phys. **36**, 3688 (1965).
[2] D. Dufft, A. Rosenfeld, S. K. Das, R. Grunwald, J. Bonse, J. Appl. Phys. **105**, 034908 (2009).
[3] J. Bonse, H. Sturm, D. Schmidt, W. Kautek, Appl. Phys. A **71**, 657 (2000).
[4] V. Oliveira, S. Ausset, R. Vilar, Appl. Surf. Sci. **255**, 7556 (2009).
[5] J. E. Sipe, J. F. Young, J. S. Preston, H. M. van Driel, Phys. Rev. B, **27**(2), (1983).
[6] A. Y. Vorobyev, V. S. Makin, Chunlei Guo, Appl. Phys. **101**, 034903 (2007).
[7] J. Bonse, J. Krüger, S. Höhm, A. Rosenfeld, J. Laser Appl. **24**(4), 042006 (2012).
[8] J. E. Sipe, J. F. Young, J. S. Preston, H. M. van Driel, Phys. Rev. B **27**, 1141 (1983).
[9] J. Bonse, A. Rosenfeld, J. Küger, J. Appl. Phys. **106**, 104910 (2009).
[10] B. Dusser, Z. Sagan, H. Soder, N. Faure, J. P. Colombier, M. Jourlin, E. Audouard, Opt. Express. **18**, 2913 (2010).
[11] A. Y. Vorobyev, C. Guo, Appl. Surf. Sci. **253**, 7272 (2007).
[12] T. Y. Hwang, A. Y. Vorobyev, C. Guo, Appl. Phys. A **108**, 299 (2012).
[13] C. Albu, A. Dinescu, M. Filipescu, M. Ulmeanu, M. Zamfirescu, Appl. Surf. Sci. **278**, 347 (2013).
[14] R. Wagner, J. Gottmann, J. Phys.: Conf. Ser. **59**, 333 (2007).
[15] M. Gedvilas, B. Voisiat, G. Račiukaitis, K. Regelskis, Appl. Surf. Sci. **255**, 9826 (2009).
[16] H. Raether, Surface Plasmons on Smooth and Rough Surfaces and on Gratings, Springer-Verlag, Berlin (1988).
[17] F. Garrelie, J. P. Colombier, F. Pigeon, S. Tonchev, N. Faure, M. Bounhalli, S. Reynaud, O. Parriaux, Opt. Exp. **19**, 9035 (2011).

*Corresponding author: catalina.radu@inflpr.ro